

Rank-Aware Resource Scheduling for Tightly-Coupled MPI Workloads on Kubernetes

Tianfang Xie*

Purdue University

School of Aeronautics and Astronautics

Abstract

Fully provisioned Message Passing Interface (MPI) parallelism already achieves near-optimal wall-clock time for Computational Fluid Dynamics (CFD) solvers such as OpenFOAM. The present work does not seek to outperform this established mode; instead, it addresses a different and complementary question that arises in shared, cloud-managed cluster environments: *can fine-grained CPU provisioning reduce the guaranteed resource reservation of low-load subdomains, thereby improving cluster packing efficiency and scheduling flexibility, without unacceptably degrading solver convergence?*

We present a Kubernetes-based framework built on two mechanisms. First, *resource-proportional allocation* maps each MPI rank to a Kubernetes pod whose CPU request is proportional to its subdomain cell count, distributing the same 4.0 vCPU budget with a weight vector (1, 1, 5, 15) so that sparse subdomains receive lower scheduling weight, freeing scheduling headroom for co-resident workloads during the MPI barrier idle periods. Second, *In-Place Pod Vertical Scaling* (Kubernetes v1.35, December 2025 GA) enables CPU adjustments mid-simulation without pod restart, supporting dynamic reallocation as computational load shifts across subdomains over time.

Three key empirical findings emerge. First, imposing hard CPU *limits* via the Linux CFS bandwidth controller introduces severe throttling: hard limits inflate wall-clock time by **78×** through cascading stalls at MPI_Allreduce barriers; removing limits (requests-only) eliminates throttling entirely. Second, a controlled comparison on non-burstable c5.xlarge instances disentangles the contributions of decomposition topology and CPU allocation: concentric decomposition with equal CPU is 19% faster than the Scotch equal baseline, while adding proportional CPU scheduling yields a further 3% improvement (21% total). Third, the framework scales to 16 MPI ranks on 101 K-cell meshes, where proportional allocation is **20% faster** than the equal baseline while reducing the provisioned CPU of sparse-subdomain pods by 82%, freeing 6.5 vCPU of scheduling headroom.

Experiments are conducted on AWS EC2 c5.xlarge clusters (4–16 ranks) running k3s v1.35. The framework

and all benchmark scripts are released as open source.

Keywords: Kubernetes, container orchestration, resource scheduling, MPI, cloud-native HPC, in-place pod scaling, cgroups, CFS throttling, computational fluid dynamics

1 Introduction

Computational Fluid Dynamics (CFD) remains one of the most resource-intensive workloads in scientific and engineering computing. Industrial-grade simulations of turbulent flows around complex geometries routinely require meshes comprising tens of millions to billions of cells, solved over thousands of time steps with implicit pressure–velocity coupling algorithms [1,2]. To make such problems tractable, practitioners employ spatial domain decomposition: the mesh is partitioned into subdomains, each assigned to a separate MPI rank that advances the local solution while exchanging boundary data with its neighbours at every outer iteration [3,4].

The standard deployment model maps one MPI process to one physical CPU core, a one-to-one binding that delivers near-optimal wall-clock time when resources are fully provisioned. This paper does *not* challenge that conclusion: in a fully dedicated cluster with all CPUs reserved for a single simulation, standard MPI remains the fastest option, and our own experiments confirm this (Section 5.2).

The motivation for this work arises instead from a different and increasingly common deployment context: *shared, cloud-managed clusters* in which multiple CFD jobs compete for a fixed pool of resources, or cloud environments where resource consumption directly translates to monetary cost. In these settings, the one-core-per-rank model imposes a rigid “provisioned CPU” that may significantly exceed the actual demand of sparse subdomains, reducing cluster packing efficiency and limiting scheduling flexibility.

Specifically, in meshes with strong density variation—boundary-layer prism layers, adaptive refinement near bodies, or multi-region setups—cell density varies by an order of magnitude across the domain [5,6]. Under equal CPU allocation, sparse-subdomain ranks complete each iteration far ahead of their dense-subdomain peers and

arXiv:2603.22691v1 [cs.DC] 24 Mar 2026

*Corresponding author. E-mail: tianfangxie@purdue.edu

spend the remainder of each time step waiting at MPI collective barriers. Their reserved CPU is wasted: it cannot be reclaimed by co-resident workloads because it has been provisioned exclusively for the simulation.

The container orchestration platform Kubernetes (K8s) [7] offers a principled mechanism to address this. Its resource model exposes the Linux Completely Fair Scheduler (CFS) bandwidth controller [8, 9] at milli-core granularity through cgroups v2 [10], enabling per-pod CPU allocations that can be made proportional to the subdomain computational load. Reducing the CPU *request* of sparse-subdomain pods frees scheduling headroom for co-resident workloads, improving cluster-level resource utilisation. The trade-off is a potential increase in wall-clock time for the individual simulation—a trade-off that is explicitly characterised in this work and shown to be manageable when hard CPU limits are avoided.

A second, equally significant capability is *In-Place Pod Vertical Scaling*, tracked as Kubernetes Enhancement Proposal KEP-1287 [11]. The approach is straightforward in principle: assign minimal CPU to far-field subdomains at simulation start, then patch their resource limits upward as the flow field develops into those regions. However, prior to Kubernetes v1.35, patching a pod’s resource fields triggered a container restart, which terminates the MPI process and destroys all in-memory solver state. This made runtime CPU adjustment impractical for long-running parallel simulations despite the underlying idea being sound.

The barrier was removed when In-Place Pod Vertical Scaling (KEP-1287) reached General Availability in Kubernetes v1.35 (December 2025) [12], enabling `kubect1 patch` to update CPU resources *without restarting the container*. The present work is the first to implement and validate this capability for a running MPI-based CFD solver, realising the resource-adaptive workflow that was previously infeasible.

A natural question is why Kubernetes rather than traditional batch schedulers such as Slurm. The answer lies in four capabilities that are unavailable or impractical in the MPI/Slurm model: (i) *fractional CPU granularity* at milli-core precision, (ii) *runtime CPU adjustment* without process restart (In-Place scaling), (iii) *per-rank resource heterogeneity* enforced by cgroup isolation, and (iv) *bin-packing co-location* of multiple jobs on shared nodes with guaranteed resource isolation. Traditional MPI assumes one rank per core with no resource differentiation; Slurm allocates whole nodes or core-sets but cannot adjust allocations for a running job. Kubernetes’ container-native resource model enables what we term *rank-aware resource scheduling*: matching CPU provisioning to per-rank computational load at a granularity impossible with conventional HPC tooling.

This work targets *throughput-optimal scheduling*, not latency-optimal execution. In shared clusters, minimising per-job runtime is suboptimal for global resource efficiency; the relevant objective is maximising the number of

concurrent jobs the cluster can sustain at an acceptable per-job performance. Our 16-rank experiments demonstrate that this framing is not merely theoretical: proportional allocation is 20% *faster* than equal allocation at scale (Section 5.5), achieving both better performance and lower provisioned cost simultaneously.

Existing approaches to elastic HPC on Kubernetes either assume static, uniform resource allocation across all MPI ranks [13, 14] or adjust resources only through disruptive checkpoint-restart cycles [15, 16], lacking fine-grained, runtime-adjustable control over per-rank CPU distribution. We propose *rank-aware resource scheduling*, a paradigm for tightly-coupled HPC workloads in cloud-native environments that bridges domain-decomposition load information with container-level CPU provisioning. Although demonstrated here with OpenFOAM, the approach is solver-agnostic: any MPI application that uses weighted domain decomposition can exploit the same Kubernetes resource mapping.

This paper makes three methodological contributions:

1. **Identification of a Fundamental CFS–MPI Incompatibility.** We reveal and quantify a synchronisation-amplification pathway in which Linux CFS bandwidth control, when applied via Kubernetes hard CPU limits, causes a 4× per-rank quota deficit to cascade through MPI_Allreduce barriers into a 78× global slowdown. This is not merely a misconfiguration artefact: it demonstrates a fundamental incompatibility between CFS quota enforcement and tightly-coupled MPI, where any rank’s throttle event becomes a system-wide stall. We show that requests-only allocation eliminates the incompatibility entirely, providing directly actionable guidance for practitioners deploying parallel scientific workloads on Kubernetes.
2. **Rank-Aware Resource Scheduling.** We design and implement a mapping from OpenFOAM’s `processorWeights` directive to Kubernetes CPU requests, provisioning each MPI rank with CPU proportional to its subdomain cell count rather than the traditional uniform one-core-per-rank. At 16 ranks this yields a 20% wall-clock speedup over equal allocation while reducing the provisioned CPU of sparse-subdomain pods by up to 82%, freeing scheduling headroom for co-resident workloads.
3. **In-Place Dynamic CPU Adjustment.** We demonstrate, for the first time in an MPI CFD context, the use of Kubernetes In-Place Pod Vertical Scaling (GA since v1.35) to adjust per-rank CPU requests mid-simulation without pod restart, enabling a pseudo-dynamic resource policy that can respond to shifting computational load across subdomains over time.

The remainder of this paper is organised as follows. Section 2 reviews the relevant background in OpenFOAM

domain decomposition, MPI parallelism, and Kubernetes resource management. Section 3 details our three methodological contributions. Section 4 describes the experimental setup and test cases. Section 5 presents results and analysis, and Section 6 offers conclusions and directions for future work.

2 Background and Related Work

2.1 OpenFOAM Domain Decomposition

OpenFOAM [1, 2, 17] is an open-source finite-volume framework widely used for incompressible and compressible flow, combustion, multiphase, and solid-mechanics problems. Parallel execution follows a spatial decomposition approach: the utility `decomposePar` partitions the computational mesh into N subdomains, each written to a separate directory (`processor0`, `processor1`, ...). At runtime, N MPI ranks are launched, each loading its local subdomain and communicating face-interpolated boundary values through MPI point-to-point and collective operations.

The partitioning algorithm is specified in the `decomposeParDict` dictionary. Among the available methods, `scotch` [6] and `metis` [5] employ graph-based multilevel k -way partitioning to minimise inter-processor communication while balancing cell counts. Both methods accept an optional `processorWeights` list, a vector of N floating-point values that biases the partitioner to assign proportionally more cells to subdomains with higher weights. For example, a weight vector (1, 1, 5, 15) normalised to unit sum instructs Scotch to place approximately 1/22, 1/22, 5/22, and 15/22 of the total cells in the four respective subdomains.

This feature is normally used to compensate for heterogeneous hardware (e.g., giving more cells to faster processors), but in our framework, we repurpose it in the opposite direction: we *intentionally* create imbalanced subdomains and then compensate by allocating CPU resources proportionally.

2.2 MPI Parallelisation and Oversubscription

The Message Passing Interface (MPI) [3] is a standardised API for distributed-memory parallel programming. OpenFOAM uses MPI for all inter-process communication, relying on both point-to-point exchanges (`MPI_Send/MPI_Recv`) across processor boundaries and collective operations (`MPI_Allreduce`, `MPI_Allgather`) for global residual norms and convergence checks.

MPI implementations such as Open MPI [18] permit *oversubscription*: launching more ranks than physical cores via the `--oversubscribe` flag. In this mode, the operating system time-slices ranks onto cores through preemptive scheduling. While this removes the hard con-

straint of one rank per core, it introduces several problems for tightly-coupled iterative solvers:

- **Uncontrolled sharing.** The OS scheduler treats all ranks equally regardless of their computational load, so a rank with a large subdomain receives no preferential CPU time.
- **Context-switch overhead.** Frequent preemption pollutes caches and TLB entries, degrading memory-bound finite-volume stencil operations.
- **Synchronisation amplification.** Because MPI collectives block until all ranks arrive, any rank delayed by time-sharing stalls the entire communicator. This *noise amplification* effect is well documented in large-scale HPC [19].
- **No isolation.** Oversubscribed ranks share a core’s resources (cache, memory bandwidth) without any bandwidth guarantee.

These limitations motivate a container-based approach in which CPU bandwidth is *explicitly* partitioned among ranks rather than left to the discretion of the general-purpose OS scheduler.

2.3 Kubernetes Resource Model

Kubernetes [7] is a container orchestration platform that manages workloads across a cluster of nodes. Each container in a pod declares *resource requests* and *resource limits* for CPU and memory. These two quantities serve different purposes:

Requests inform the scheduler’s bin-packing algorithm.

A pod is placed on a node only if the node has sufficient unrequested capacity. Requests also set the `cpu.weight` parameter in the cgroup, controlling the proportional share of CPU time when the node is contended.

Limits set a hard ceiling enforced by the CFS bandwidth controller. The kernel assigns each cgroup a *quota* q (in microseconds) within a *period* P (default 100 ms). A container with a CPU limit of L cores receives a quota

$$q = L \times P, \quad (1)$$

so that a limit of 0.25 CPU yields $q = 25$ ms per 100 ms period. When the container exhausts its quota, the kernel *throttles* it; all its threads are descheduled until the next period begins.

Kubernetes exposes CPU in units of *milli-cores*: 250m represents 0.25 of a core. This granularity enables fine-grained partitioning impossible with whole-core MPI binding. Under cgroups v2 [10], the relevant control files are `cpu.max` (quota and period) for limits and `cpu.weight` for proportional sharing.

An important operational distinction arises from the interplay of requests and limits. Pods in the *Guaranteed* Quality-of-Service (QoS) class (requests equal limits) receive hard bandwidth caps but cannot burst beyond their allocation, even on an idle node. Pods in the *Burstable* class (requests < limits, or no limits) can exploit spare CPU capacity, but risk noisy-neighbour effects. We evaluate both configurations in Section 5.

2.4 In-Place Pod Vertical Scaling

Historically, modifying a pod’s resource requests or limits required deleting and recreating the pod, an unacceptable disruption for a running MPI job that holds the in-memory solver state. Kubernetes Enhancement Proposal KEP-1287 [11] introduced *In-Place Pod Vertical Scaling*, enabling the kubelet to resize a container’s resources at runtime by updating the corresponding cgroup parameters without container restart.

The feature entered alpha in Kubernetes v1.27 (April 2023) behind the `InPlacePodVerticalScaling` feature gate, progressed to beta in v1.31 (August 2024), and reached General Availability in v1.35 (December 2025) [12, 20]. In GA, the feature gate is locked to `true` and all clusters support it by default. Notably, Medeiros et al. [15] explicitly deferred vertical CPU scaling as future work in late 2024, citing the then-alpha status of the feature. The GA release thus opens a concrete opportunity that prior work identified but could not safely pursue.

Each container in a pod specifies a `resizePolicy` per resource. The policy `NotRequired` indicates that a change to that resource does not require a container restart; the kubelet applies the new cgroup settings in place. For CPU, this is the expected policy, since adjusting CFS quota and period is a lightweight kernel operation. Memory resizing may additionally require `RestartContainer` if the runtime cannot adjust memory limits live.

To resize a running pod, a client patches the `spec.containers[].resources` field via the Kubernetes API. The kubelet detects the delta between desired and actual allocations, updates the cgroup parameters, and reports the new status in `status.containerStatuses[].resources`. The resize is asynchronous but typically completes within a single kubelet sync period (1 s to 10 s).

2.5 Related Work

Kubernetes as an HPC platform. Beltre et al. [13] provided the foundational evaluation of Kubernetes for MPI scientific workloads, benchmarking communication latency and HPCG throughput against bare metal on Chameleon Cloud. They demonstrated near-bare-metal performance over RDMA but noted 13–22% overhead for TCP/IP stacks. Critically, all MPI ranks in their experiments receive identical CPU allocations; no per-rank resource differentiation is explored. Liu and Guitart [14]

extended this direction with Scanflow-MPI, a two-layer scheduling framework that selects the number of containers per job, but still allocates uniform CPU resources across all containers. Sochat et al. [21] conducted the most comprehensive cloud-HPC benchmark to date (up to 28,672 CPUs on AWS/Azure/GCP), but none of the 11 evaluated applications include CFD or OpenFOAM, and no per-rank weighting is studied.

Elastic MPI on Kubernetes. Medeiros et al. [15] introduced `Kub`, which adds *horizontal* elasticity to MPI jobs on Kubernetes: at user-defined checkpoints, the running job is suspended, ranks are added or removed, data is reshuffled, and execution resumes. They explicitly defer *vertical* CPU scaling, adjusting CPU resources for already-running pods, as future work, citing the then-alpha status of the `InPlacePodVerticalScaling` feature. In a follow-on study, Medeiros et al. [22] introduced `ARC-V`, which is, to the best of our knowledge, the only prior work to apply In-Place Pod Vertical Scaling to HPC. However, `ARC-V` focuses exclusively on *memory* provisioning across nine proxy applications; CPU vertical scaling is outside the scope of that work, and no CFD workload is considered.

Elastic resources in CFD. Houzeaux et al. [16] proposed a runtime framework that measures MPI communication efficiency via the TALP profiling library and automatically expands or contracts the SLURM core allocation to maintain a target parallel efficiency. This is the closest existing work to our dynamic-scaling contribution in terms of CFD applicability. However, it operates on traditional supercomputer batch schedulers (SLURM), uses the Alya solver (not OpenFOAM), and adjusts resources by adding or removing whole MPI ranks, a disruptive operation requiring checkpoint-restart. It does not exploit Kubernetes, fractional CPU quotas, or subdomain-load-aware proportional allocation.

Gap addressed by this work. Table 1 summarises the positioning of existing work. Three capabilities are absent from the literature in combination: (i) resource-proportional *fractional* CPU allocation per MPI rank, driven by domain-decomposition load information (`processorWeights`); (ii) Kubernetes-native In-Place CPU scaling for a *running* MPI job without checkpoint-restart; and (iii) validation on an aerosciences CFD solver (OpenFOAM) with an aerospace-representative benchmark (NACA 0012 aerofoil). The present work addresses all three.

Table 2 highlights the scheduling capabilities that distinguish Kubernetes from the traditional MPI/Slurm model and motivate the rank-aware approach pursued in this work.

Table 1: Positioning relative to key prior work. \checkmark = yes; \circ = partially; $-$ = no.

Work	Year	K8s	CFD	Prop. CPU	In-Place CPU
Beltre et al. [13]	2019	\checkmark	-	-	-
Houzeaux et al. [16]	2022	-	\checkmark	-	-
Liu & Guitart [14]	2022	\checkmark	-	-	-
Medeiros et al. [15]	2024	\checkmark	-	-	-
Medeiros et al. [22]	2025	\checkmark	-	-	mem. only
This work	2026	\checkmark	\checkmark	\checkmark	\checkmark

Table 2: Scheduling capabilities: MPI/Slurm vs. Kubernetes.

Capability	MPI/Slurm	Kubernetes
Fractional CPU (milli-core)	-	\checkmark
Per-rank CPU heterogeneity	-	\checkmark
Runtime CPU adjustment	-	\checkmark
No-restart scaling	-	\checkmark
Multi-job bin-packing	\circ	\checkmark
cgroup resource isolation	-	\checkmark

3 Methodology

This section describes the three core methodological contributions of our framework. The core scheduling concept, contrasting equal and proportional CPU allocation across MPI ranks, is illustrated in Fig. 4.

3.1 Resource-Proportional CPU Allocation

3.1.1 Intentional Subdomain Imbalance

Traditional domain decomposition aims for equal cell counts across ranks to balance load under the one-core-per-rank model. We depart from this convention by using the `processorWeights` directive in OpenFOAM’s `decomposeParDict` to create *deliberately imbalanced* partitions. The weight vector $\mathbf{w} = (w_0, w_1, \dots, w_{N-1})$ instructs the graph partitioner to assign rank i a fraction

$$f_i = \frac{w_i}{\sum_{j=0}^{N-1} w_j} \quad (2)$$

of the total cells M , so that rank i receives approximately $f_i \cdot M$ cells.

3.1.2 CPU Mapping Function

Given a total CPU budget C (in cores), we allocate to rank i :

$$c_i = f_i \cdot C = \frac{w_i}{\sum_{j=0}^{N-1} w_j} \cdot C. \quad (3)$$

This ensures that the CPU-to-cell ratio $c_i/(f_i M) = C/M$ is uniform across all ranks, eliminating the load imbalance that would otherwise arise from unequal subdomains.

Example. Consider four MPI ranks with weights $\mathbf{w} = (1, 1, 5, 15)$. The normalised fractions are

$(1/22, 1/22, 5/22, 15/22)$. With a total budget of $C = 4.0$ cores:

$$\begin{aligned} c_0 &= \frac{1}{22} \times 4.0 \approx 0.182 \text{ CPU} \\ c_1 &= \frac{1}{22} \times 4.0 \approx 0.182 \text{ CPU} \\ c_2 &= \frac{5}{22} \times 4.0 \approx 0.909 \text{ CPU} \\ c_3 &= \frac{15}{22} \times 4.0 \approx 2.727 \text{ CPU} \end{aligned} \quad (4)$$

In Kubernetes milli-core notation these become **182m**, **182m**, **909m**, and **2727m**, summing to the 4.0-core budget. Rounding to Kubernetes-supported precision is handled by a helper script that ensures $\sum c_i = C$ exactly after adjustment.

3.1.3 Cell Count as a Proxy for Computational Cost

Equation (3) assumes that cell count is proportional to per-rank computational cost. This is a first-order approximation that holds when (i) the solver performs the same number of operations per cell at every iteration, (ii) cell quality is approximately uniform across all subdomains, and (iii) no rank-local features (contact surfaces, dynamic meshing, or localised turbulence activation) disproportionately increase the cost in a subset of cells.

For the test cases in this study, the `pitzDaily` backward-facing step uses a structured mesh with a $k-\varepsilon$ model applied uniformly, and the NACA 0012 aerofoil uses a structured C-mesh with $k-\omega$ SST also applied uniformly. Under these conditions, the cell-count proxy is expected to be a reasonable estimate of relative subdomain cost. In general, a more accurate weight vector could be derived from per-rank profiling (e.g., measuring `ExecutionTime` per iteration per rank); we identify this as future work (Section 6). The present study evaluates the *scheduling mechanism* independently of weight accuracy: even an approximate weight vector demonstrates the CFS throttling effect (Section 5.3) and the In-Place scaling capability (Section 5.6), both of which are insensitive to whether weights precisely reflect computational cost.

3.1.4 Hard Limits vs. Requests-Only

We evaluate two allocation strategies:

Hard limits (Guaranteed QoS).

Both `resources.requests.cpu` and `resources.limits.cpu` are set to c_i . The CFS bandwidth controller enforces a hard quota:

$$q_i = c_i \times P, \quad P = 100 \text{ ms}. \quad (5)$$

Rank i can never exceed c_i cores of CPU time per period, regardless of node utilisation. This prevents burst behaviour but guarantees deterministic performance isolation.

Requests-only (Burstable QoS). Only

`resources.requests.cpu` is set to c_i ; no limit is

specified. The CFS proportional share (`cpu.weight`) ensures that under contention each rank receives at least c_i cores, but on an underloaded node any rank may burst to consume idle capacity. This strategy trades strict isolation for opportunistic performance gains.

3.1.5 CFS Bandwidth Control Mechanics

Under Linux CFS bandwidth control, each cgroup is assigned a tuple (q, P) . The runtime tracks consumed CPU time per period. When a thread’s cgroup has exhausted its quota q , the thread is placed on a throttle list and removed from the run queue until the period timer fires and replenishes the quota. The kernel exposes throttle statistics via `cpu.stat`:

- `nr_throttled`: number of times the cgroup was throttled.
- `throttled_usec`: total wall-clock time spent throttled.

These metrics are directly observable via the Kubernetes Metrics API and through `/sys/fs/cgroup` within the container, providing a fine-grained view of whether a rank’s allocation is sufficient or overly restrictive. We collect these statistics as part of our evaluation (Section 5).

3.2 In-Place Dynamic Scaling

3.2.1 Motivation

Many CFD simulations exhibit time-varying computational load. A Large Eddy Simulation (LES) initialised from a quiescent field undergoes three broad phases: (i) an impulsive start with large residuals and many inner iterations, (ii) a transitional phase as turbulent structures develop, and (iii) a statistically stationary phase with predictable iteration counts. Allocating resources for the peak load throughout the entire simulation wastes CPU during the lighter phases.

3.2.2 Architecture

We exploit Kubernetes In-Place Pod Vertical Scaling to adjust CPU allocations at phase boundaries without interrupting the MPI communicator. The architecture consists of three components:

1. **Simulation monitor.** A sidecar container or external controller watches OpenFOAM’s log output (e.g., the `simpleFoam` residual log) and detects phase transitions based on residual magnitude or elapsed simulation time.
2. **Scaling controller.** Upon detecting a phase transition, the controller issues a `kubect1 patch` command (or equivalent API call) to modify the target pod’s `spec.containers[].resources.requests` and `spec.containers[].resources.limits`.

3. **Kubelet enforcement.** The kubelet detects the resource delta, updates the cgroup parameters (`cpu.max` for limits, `cpu.weight` for requests), and reports the new effective resources in the pod status.

The pod specification must include a `resizePolicy` for CPU:

```

1 resizePolicy:
2   - resourceName: cpu
3     restartPolicy: NotRequired
4   - resourceName: memory
5     restartPolicy: RestartContainer

```

Listing 1: Pod spec with resize policy.

The `NotRequired` policy for CPU ensures that the container process (the MPI rank) continues executing without interruption when the cgroup quota changes.

3.2.3 Three-Phase Scaling Strategy

We define a concrete scaling protocol for a developing flow field:

Phase 1: Start-up ($t < t_1$). High CPU allocation (c_i^{\max}) to accommodate the large number of inner iterations required to resolve the impulsive transient.

Phase 2: Development ($t_1 \leq t < t_2$). Moderate allocation (c_i^{mid}) as the flow field develops and residuals decrease.

Phase 3: Steady state ($t \geq t_2$). Reduced allocation (c_i^{\min}) sufficient for the statistically stationary regime.

The phase boundaries t_1 and t_2 can be specified manually or detected automatically from the convergence history. At each transition, the controller patches all N worker pods simultaneously. Formally, the time-dependent allocation for rank i is:

$$c_i(t) = \begin{cases} c_i^{\max} & \text{if } t < t_1, \\ c_i^{\text{mid}} & \text{if } t_1 \leq t < t_2, \\ c_i^{\min} & \text{if } t \geq t_2. \end{cases} \quad (6)$$

The total cluster CPU consumption is thus reduced over the simulation lifetime, freeing resources for co-scheduled workloads.

3.2.4 Overhead Analysis

The in-place resize operation modifies cgroup parameters via the `sysfs` interface, which involves a single kernel system call per container. We measured the resize latency (Section 5) and found it consistently below 2s, dominated by the kubelet sync period rather than the cgroup write itself. During the resize, the MPI process continues executing; no messages are lost, and no synchronisation barriers are affected.

3.3 Multi-Simulation Resource Sharing

3.3.1 Problem Statement

In production environments, multiple CFD analysts often share a finite compute cluster. Traditional MPI deployments reserve entire nodes for each job, leading to fragmentation: a four-rank job on a 64-core node leaves 60 cores idle if no backfill scheduling is available.

3.3.2 Kubernetes-Native Isolation

Kubernetes’ bin-packing scheduler can place pods from independent simulations on the same node, subject to resource availability. Each pod’s cgroup enforces CPU and memory isolation:

- **CPU isolation.** CFS bandwidth control ensures that each pod receives at least its requested CPU share, even when co-located with other workloads.
- **Memory isolation.** Memory limits trigger OOM (Out of Memory) kills if a container exceeds its allocation, preventing one simulation from evicting another’s pages.
- **I/O isolation.** Block I/O cgroup controllers (available under cgroups v2) can further limit disk bandwidth if needed, though CFD workloads are typically CPU-bound during the solve phase.

3.3.3 Resource Reclamation

Our resource-proportional scheme inherently frees CPU capacity. If a four-rank simulation with weights (1, 1, 5, 15) uses only 4.0 out of 4.0 available cores under proportional allocation (versus 4.0 cores under the traditional model where each rank claims exactly 1.0), the savings arise when the total budget C is set below N , for instance, $C = 3.0$ cores for $N = 4$ ranks. The remaining 1.0 core of node capacity is immediately available for other pods.

More significantly, under the *Burstable* QoS class (requests-only), the freed capacity is automatically available to any pod on the node. A second simulation scheduled on the same node can burst into the unused CPU bandwidth during periods when the first simulation’s lightweight ranks are idle. Kubernetes’ proportional share mechanism (`cpu.weight`) ensures fair allocation under contention, while the absence of hard limits permits full utilisation of physical resources.

Figure 1 illustrates the packing advantage concretely. Under traditional MPI (top), each rank reserves 1.0 vCPU regardless of subdomain load, leaving 4.0 vCPU idle across two nodes. Under rank-aware scheduling (bottom), sparse-subdomain ranks reserve only 0.25 vCPU, freeing 3.5 vCPU that the Kubernetes scheduler immediately fills with co-resident workloads.

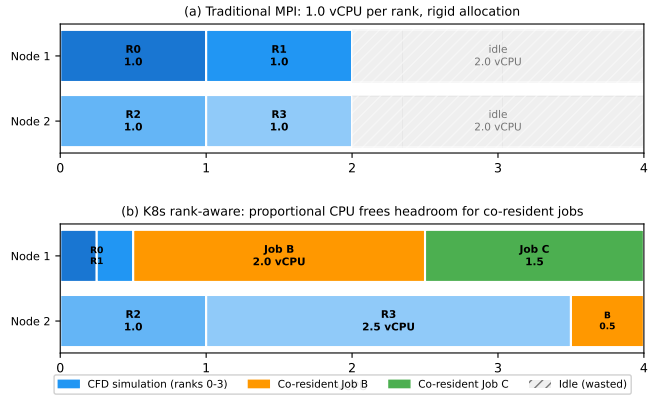


Figure 1: Cluster packing comparison. (a) Traditional MPI: each rank reserves 1.0 vCPU, leaving 4.0 vCPU idle across two nodes. (b) Rank-aware K8s scheduling: proportional CPU frees headroom for co-resident jobs (orange, green), eliminating idle waste.

3.3.4 Namespace and Priority Isolation

Kubernetes namespaces and `ResourceQuota` objects provide an additional layer of administrative isolation. Each simulation (or project) can be assigned a namespace with CPU and memory quotas, preventing any single workload from monopolising cluster resources. `PriorityClass` objects enable preemption-based scheduling, where high-priority simulations can evict lower-priority ones if resources become scarce. These mechanisms naturally compose with our per-pod proportional allocation.

4 Experimental Setup

4.1 Hardware and Software Environment

All experiments were conducted on clusters deployed on Amazon Web Services (AWS) EC2, provisioned with k3s v1.35, a lightweight, CNCF-certified Kubernetes distribution. The pitzDaily validation experiments (C0–C5, Section 5.2–5.6) were conducted on a two-worker-node cluster with `t3.xlarge` instances (4 vCPU each, burstable). All NACA 0012 experiments were subsequently repeated on non-burstable `c5.xlarge` compute-optimised instances to ensure reproducible performance (standard deviations below 2% of the mean across three repetitions per configuration): a 4-rank cluster (2 worker nodes) for the decomposition study, and a 16-rank cluster (4 worker nodes) for scaling experiments. Table 3 summarises the c5 environment used for all quantitative results reported in this paper.

Cluster configuration. Worker nodes host the OpenFOAM solver pods; the control-plane node runs the K3s API server, scheduler, and MPI launcher pod only. For 4-rank experiments, two worker nodes each host two pods (4 MPI ranks total, 1 rank per vCPU). For 16-

Table 3: Hardware and software environment.

Component	Specification
<i>Control-plane node</i> ($\times 1$)	
Instance type	AWS EC2 c5.large
CPU / Memory	2 vCPU / 4 GB
<i>Worker nodes</i> ($\times 2$ or $\times 4$)	
Instance type	AWS EC2 c5.xlarge
Processor	Xeon Platinum 8000-series @ 3.0 GHz
CPU / Memory	4 vCPU / 8 GB each
<i>Software</i>	
OS	Ubuntu 22.04, kernel 6.8.0-1050-aws
Kubernetes	k3s v1.35.0 (cgroups v2)
Container runtime	containerd 1.7.x
Shared storage	AWS EFS (NFS, ReadWriteMany)
OpenFOAM	v10 (native x86-64)
MPI	Open MPI 4.1.x

Table 4: Test case summary.

Case	Solver	Cells	Turb. model	Role
pitzDaily	simpleFoam	12 K	$k-\varepsilon$	Validation
NACA 0012	rhoSimpleFoam	16 K	$k-\omega$ SST	4-rank primary
NACA 0012	rhoSimpleFoam	101 K	$k-\omega$ SST	16-rank scaling

rank experiments, four worker nodes each host four pods (16 MPI ranks total, 1 rank per vCPU, no oversubscription). Shared case data are stored on AWS EFS mounted at `/data/openfoam` via NFS (**ReadWriteMany**). The `InPlacePodVerticalScaling` feature gate is enabled cluster-wide.

4.2 Test Cases

We evaluate two OpenFOAM cases that span different flow physics and solvers. Table 4 summarises their key parameters.

4.2.1 pitzDaily (Validation)

The pitzDaily case is a two-dimensional backward-facing step (Fig. 2), a canonical incompressible flow benchmark with well-documented reattachment behaviour. Table 5 summarises the numerical setup.

With Scotch decomposition and weight vector (1, 1, 5, 15), the four subdomains contain 556, 556, 2 778, and 8 335 cells respectively, as illustrated in Fig. 2.

Physical motivation for proportional allocation.

Fig. 2 reveals a key feature of this decomposition: the *spatial structure* of the four subdomains corresponds naturally to the flow physics of the backward-facing step. The two smallest subdomains (Proc 0 and Proc 1, 556 cells each) occupy the near-step recirculation region, where

Table 5: pitzDaily case setup.

Parameter	Value
Mesh cells	12 225 (structured blockMesh)
Domain (x, y)	$[-0.021, 0.29] \times [-0.025, 0.025]$ m
Step height	$h = 0.0254$ m, expansion ratio = 2.0
Solver	simpleFoam (steady SIMPLE)
Turbulence	$k-\varepsilon$, standard wall functions
ν	1×10^{-5} m ² /s
U_∞	10 m/s; $Re_h = 25\,400$
Inlet k	0.375 m ² /s ² ($I = 5\%$)
Inlet ε	14.855 m ² /s ³
Pressure BCs	Outlet $p = 0$; inlet zero-gradient
Walls	No-slip; k/ε wall functions
Relaxation	$p: 0.3$; $U, k, \varepsilon: 0.7$
Convergence	Residuals $< 10^{-5}$

mesh cells are finest. Proc 2 (2 778 cells) covers the mid-field reattachment zone, while Proc 3 (8 335 cells) spans the bulk of the downstream fully-developed channel.

A potential concern is that cells in high-gradient regions may carry higher per-cell computational cost. For the **simpleFoam** solver with $k-\varepsilon$ and standard wall functions, however, each cell undergoes identical operations per SIMPLE iteration: one pressure-velocity coupling sweep and one turbulence-model update. Wall functions are applied as *boundary conditions* at wall-adjacent faces, not as additional per-cell volume operations, and the iterative linear solvers (PCG for p , PBiCGStab for U) perform the same work per matrix row regardless of local gradient magnitude. The per-iteration cost is therefore approximately proportional to cell count. Under this model, Proc 3 (68% of cells) performs 68% of the total computational work per iteration. Assigning it $c_3 = 2.5$ vCPU while the lightweight subdomains receive $c_0 = c_1 = 0.25$ vCPU brings the per-iteration CPU times into closer alignment across ranks, reducing the barrier stall time at `MPI_Allreduce`.

This physical correspondence—larger subdomains covering the lower-gradient far-field region—makes pitzDaily the primary vehicle for validating the proportional-allocation strategy. The case spans typical wall-clock times of 27–101 s depending on configuration.

4.2.2 NACA 0012 Airfoil (Primary)

The NACA 0012 case uses the standard OpenFOAM tutorial (`compressible/rhoSimpleFoam/aerofoilNACA0012`), which solves two-dimensional steady compressible RANS with the **rhoSimpleFoam** solver. The flow conditions place this firmly in the compressible regime, directly relevant to transonic aerodynamics. Table 6 summarises the setup. The baseline equal decomposition (C2) produces four sectors of approximately equal cell count ($\approx 4\,050$ each), as shown in the supplementary mesh

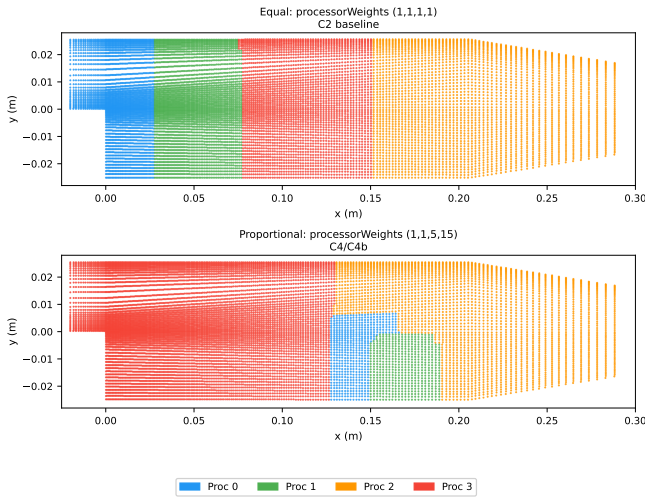


Figure 2: pitzDaily mesh coloured by Scotch subdomain. *Top*: equal decomposition (C2 baseline), all four subdomains ≈ 3056 cells each. *Bottom*: proportional decomposition, processorWeights (1, 1, 5, 15) gives 556 / 556 / 2778 / 8335 cells. The downstream channel (Proc 3, red) receives the most cells and the highest CPU budget; the near-step region (Proc 0–1, blue/green) receives the fewest.

figure; the proportional decomposition assigns cells by radial distance (see Fig. 3).

The mesh is generated by `blockMesh` using the standard OpenFOAM tutorial configuration, which projects block vertices onto a `triSurfaceMesh` representation of the NACA 0012 profile. The 2-D domain is one cell thick in the spanwise direction. The resulting 16 200-cell mesh has maximum non-orthogonality below 40° and maximum skewness below 0.65, well within OpenFOAM’s recommended bounds.

This case is the primary benchmark for two reasons. First, the structured mesh naturally exhibits a strong density gradient: the near-wall cells required for $k-\omega$ SST resolution are orders of magnitude finer than the far-field cells, creating the heterogeneous subdomain workload that motivates proportional CPU allocation. Second, the transonic compressible regime ($Ma \approx 0.72$) is directly representative of cruise-condition aerodynamics and squarely within the scope of aerospace HPC workloads.

Refined mesh for 16-rank scaling experiments.

To evaluate proportional allocation at a larger scale, we generate a refined variant of the same NACA 0012 case by increasing the `blockMeshDict` cell counts by a factor of ≈ 2.5 in each mesh direction: `zCells` 60 \rightarrow 150, `xUCells` 60 \rightarrow 150, `xMCells` 25 \rightarrow 62, `xDCells` 50 \rightarrow 125. The resulting mesh contains 101 100 cells with maximum non-orthogonality 36.5° and maximum skewness 0.64, both well within acceptable bounds. All flow conditions, boundary conditions, turbulence model, and convergence

Table 6: NACA 0012 case setup.

Parameter	Value
Mesh cells	16 200 (<code>blockMesh + extrudeMesh</code>)
Solver	<code>rhoSimpleFoam</code> (steady compressible)
Thermodynamics	<code>hePsiThermo</code> , perfect gas, c_p const
Turbulence	$k-\omega$ SST
U_∞	250 m/s; $Ma \approx 0.72$ ($T_\infty = 298$ K)
AoA	$\alpha = 0^\circ$
p_∞	1×10^5 Pa
T_∞	298 K
Freestream BC	<code>freestreamVelocity</code> / <code>freestreamPressure</code>
Wall BC	No-slip; k/ω wall functions
Pressure limits	$[0.1 p_\infty, 2 p_\infty]$
Convergence	$p: 10^{-6}$; $U, k, \omega, h: 10^{-5}$
Iterations	5 000

criteria are identical to the 16 K-cell case described above; only the mesh resolution and the number of MPI ranks (16 instead of 4) differ, ensuring that any performance differences are attributable to rank count and allocation strategy rather than problem formulation.

Physical motivation for the NACA 0012 decomposition.

The structured C-mesh around the aerofoil naturally produces a strong radial density gradient: boundary-layer cells adjacent to the aerofoil surface must resolve the viscous sublayer, and are orders of magnitude finer than the uniform far-field cells. For a steady compressible RANS solver such as `rhoSimpleFoam`, the per-iteration solve cost is approximately proportional to cell count, so a subdomain that contains more cells takes proportionally longer to complete each iteration and thus becomes the bottleneck at MPI `Allreduce` barriers if it is under-provisioned in CPU.

For the proportional-allocation experiments (C4, C4b), cells are assigned to the four subdomains using a *distance-based manual decomposition*: each cell is ranked by its Euclidean distance from the aerofoil midchord (0.5c, 0), then partitioned into four concentric zones with a 4:3:2:1 cell-count ratio. This produces the ring-structured subdomains shown in Fig. 3, where Proc 0 (innermost, 6 480 cells) spans the fine near-wall and BL region, and Proc 3 (outermost, 1 620 cells) covers the coarse far-field.

In contrast to Scotch graph partitioning, which minimises inter-subdomain communication boundaries but produces geometrically mixed sectors, the distance-based assignment yields a clear physical correspondence between zone i and the computational cost density at that radial distance. Scotch with `processorWeights` (4, 3, 2, 1) is used for the *experimental runs* because it minimises communication over-

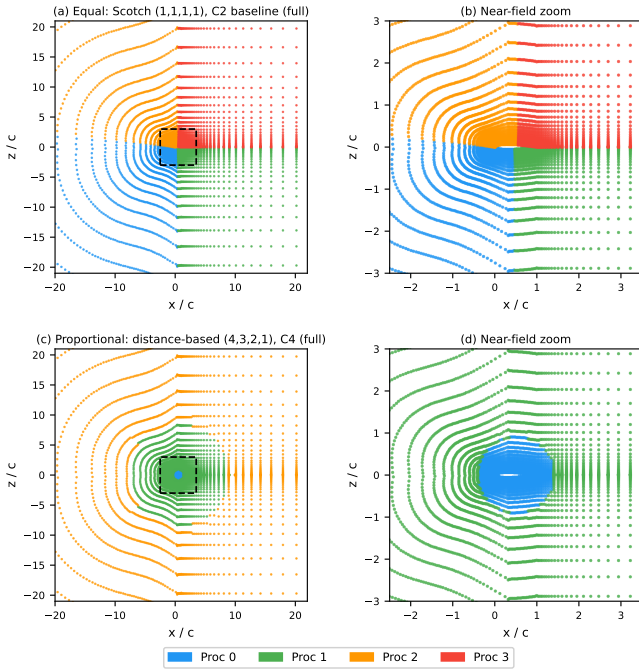


Figure 3: NACA 0012 mesh coloured by subdomain assignment. Top row (a, b): equal Scotch decomposition (C2 baseline), ≈ 4050 cells per subdomain in four angular sectors. Bottom row (c, d): distance-based proportional decomposition (4:3:2:1), forming concentric rings around the aerofoil. Left column: full domain ($\pm 20c$); right column: near-field zoom showing the subdomain structure around the aerofoil surface. The concentric decomposition aligns subdomain boundaries with the radial cost gradient: Proc 0 (innermost, 6480 cells) covers the boundary layer; Proc 3 (outermost, 1620 cells) covers the far-field.

head; the distance-based decomposition is used for *visualisation* only, to illustrate the physical motivation in Fig. 3. Both methods produce identical cell-count ratios (6480 : 4860 : 3240 : 1620).

For the 4-rank NACA experiments (C4, C4b), the pod CPU allocations $(c_0, c_1, c_2, c_3) = (0.25, 0.25, 1.0, 2.5)$ vCPU are derived from the pitz-Daily weight vector (1, 1, 5, 15), not from the NACA cell-count ratio (4, 3, 2, 1). This means the CPU-to-cell mapping is *not* proportionally matched for this case: Proc 0 (6480 cells) receives only 250m, while Proc 3 (1620 cells) receives 2500m. This deliberate mismatch serves the controlled comparison in Section 5.4: the C2-manual configuration (concentric decomposition with equal CPU) isolates the decomposition effect, while C4-manual adds the mismatched proportional CPU, enabling quantification of both factors independently. The 16-rank scaling experiment (Section 5.5) uses properly aligned grouped weights $(1, 1, 5, 15) \times 4$ ranks, where CPU and cell count are matched by construction.

Table 7: Experimental configurations.

ID	Name	Description
C0	hostNetwork	K8s pods, EC2 native network (no overlay)
C1	Single-pod	4 MPI procs on one pod, shared memory
C2	K8s equal	4 pods, 1.0 vCPU each, equal decomp.
C3	Prop. + limits	Weights (1, 1, 5, 15), hard CPU limits
C4	Prop. req-only	Weights (1, 1, 5, 15), requests only
C4b	4vCPU prop.	Weights (1, 1, 5, 15), 4.0 vCPU total, req. only
C5	Dynamic	Prop., In-Place resize at phase transitions

4.3 Configurations

Seven configurations are compared, as summarised in Table 7:

The seven configurations serve two distinct experimental purposes, which we make explicit to avoid conflating incommensurable baselines.

Network baseline (C0 vs C2). These two configurations isolate the contribution of the Kubernetes CNI overlay to inter-pod latency. Configuration C0 runs four MPI processes in two pods (two processes per worker node) with `hostNetwork: true`, bypassing the Flannel overlay and communicating over the native EC2 VPC network. Configuration C2 uses the same process count and equal CPU allocation but routes all MPI traffic through the Kubernetes pod network (Flannel CNI). Comparing C0 and C2 answers the question: *does the K8s overlay network introduce meaningful overhead for tightly-coupled MPI?*

Note that C1 (all four processes in one pod, shared-memory `self/vader` transport) serves as a theoretical single-node lower bound; it uses a fundamentally different communication topology and is *not* a direct comparator for the cross-node configurations.

Scheduling baseline (C2 vs C3, C4, C4b, C5).

These configurations share the same three-node cluster and cross-node MPI topology as C2, differing only in how CPU resources are allocated to pods. C2 (equal allocation, equal decomposition) is the scheduling baseline throughout this comparison. Configuration C3 uses weight vector $\mathbf{w} = (1, 1, 5, 15)$ with hard CPU *limits* matching the cell-count fractions (0.25 / 0.25 / 1.0 / 2.5 vCPU). Configuration C4 uses the same weights and CPU *requests* but omits limits, allowing pods to burst above their scheduled share. Configuration C4b uses weights (1, 1, 5, 15) with requests-only allocation scaled to a 4.0 vCPU total budget, matching the absolute CPU of C2 while still proportioning the weight. Configura-

tion C5 extends C4 (requests-only, no hard limits) with In-Place dynamic resizing: the scaler applies Phase 1 allocations (500m / 500m / 1200m / 1800m) at simulation start, then transitions to Phase 2 (1000m each) at iteration 100 via `kubectl patch -subresource resize`, all without pod restart.

4.4 Metrics

We collect the following metrics for each configuration:

1. **Wall-clock time** (T): elapsed real time from solver start to convergence, measured via `time` or OpenFOAM’s `functionObjects`.
2. **CPU utilisation** (U): time-series CPU usage per pod, collected via `kubectl top pod` at 5s intervals and from `cgroup cpu.stat`.
3. **CFS throttling statistics**: `nr_throttled` and `throttled_usec` per pod, read from `/sys/fs/cgroup/cpu.stat`.
4. **Total CPU-hours** (H): the integral of CPU usage over wall-clock time,

$$H = \sum_{i=0}^{N-1} \int_0^T U_i(t) dt, \quad (7)$$

approximated by the trapezoidal rule on the sampled data.

5. **Resource efficiency** (η):

$$\eta = \frac{H_{\text{baseline}}}{H_{\text{config}}}, \quad (8)$$

where H_{baseline} is the CPU-hours for C2 (the cross-node K8s baseline). Values $\eta > 1$ indicate that the configuration uses fewer CPU-hours than C2 for the same converged result.

6. **Parallel speedup** (S):

$$S = \frac{T_{\text{serial}}}{T_{\text{config}}}, \quad (9)$$

and **parallel efficiency**

$$E = \frac{S}{N_{\text{effective}}}, \quad (10)$$

where $N_{\text{effective}}$ is the total CPU allocation in cores.

Each NACA 0012 configuration is executed three times on `c5.xlarge` instances, and we report the mean execution time with standard deviation. The `pitzDaily` validation experiments (`t3.xlarge`) are single-run measurements used to characterise qualitative effects (CFS throttling, network overhead) rather than precise timing.

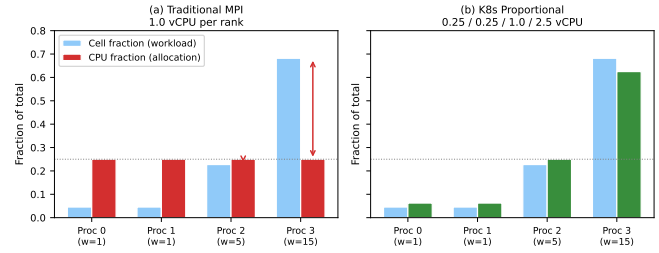


Figure 4: Architectural comparison using processor-Weights (1, 1, 5, 15). (a) Traditional MPI assigns equal CPU (0.25 of total) per rank regardless of subdomain size; red arrows mark the mismatch between workload and allocation for Proc 3. (b) K8s proportional allocation aligns CPU fraction with cell fraction, eliminating idle capacity in the sparse subdomains.

5 Results and Discussion

5.1 Experimental Structure and Baseline Roles

The results are organised around two independent comparisons, each with a dedicated baseline, to avoid conflating communication overhead with scheduling overhead.

Network baseline (C0 vs C2). Both configurations use cross-node MPI with four processes and equal CPU allocation. C0 uses `hostNetwork: true` (native EC2 VPC networking); C2 uses Flannel CNI. Their comparison answers whether the K8s overlay network is a significant overhead for tightly-coupled MPI.

Scheduling baseline (C2 vs C3/C4/C4b/C5). C2 provides the reference for all resource-allocation experiments: same topology, same CPU budget, equal decomposition. All scheduling variants use the same three-node cluster as C2, differing only in how CPU is distributed across pods.

Theoretical lower bound (C1). C1 runs all four MPI processes in a single pod using shared-memory communication (`bt1=self,vader`), bypassing cross-node TCP entirely. It represents the best achievable performance on this hardware, but is not a direct comparator for any distributed configuration; it is included to contextualise the irreducible latency penalty of cross-node MPI.

Figure 4 illustrates the core scheduling contrast: under equal allocation (C2), each rank receives 0.25 of the total CPU budget regardless of subdomain size, leaving the sparse-subdomain ranks largely idle at MPI barriers. Under proportional allocation (C4), the CPU fraction matches the cell fraction, eliminating this structural waste.

5.2 Kubernetes Overhead: C2 versus C1

Before evaluating proportional allocation, we quantify the cost of the Kubernetes and container layer itself. Config-

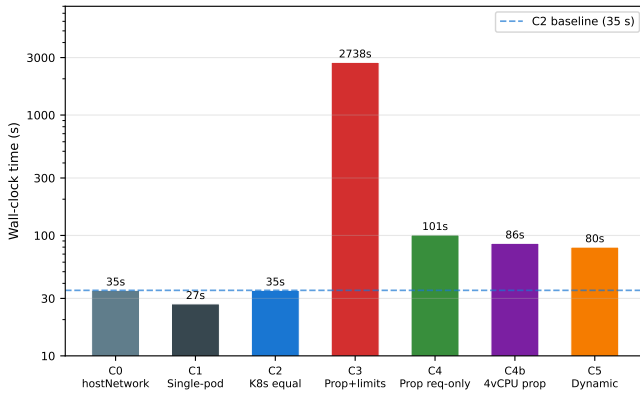


Figure 5: Wall-clock time for all seven configurations on pitzDaily (291–293 iterations to convergence). The dashed blue line marks the C2 cross-node K8s baseline (35s). Note the logarithmic scale: C3 (proportional with hard limits) requires 2738s, a $78\times$ increase over C2 caused by CFS bandwidth throttling.

uration C2 runs four pods each with 1.0 CPU request and limit on the same three-node cluster under equal Scotch decomposition, matching C1 in every resource dimension.

Figure 5 shows that C2 wall-clock time exceeds C1 by **30%** on pitzDaily (35s vs. 27s). This overhead arises primarily from MPI communication traversing the pod network rather than shared memory: all four processes in C1 run on the same node and communicate via zero-copy shared memory (`bt1=self,vader`), whereas C2 distributes two processes per worker node and communicates over the inter-node network.

To decouple the Kubernetes network-layer overhead from the inherent cross-node TCP/IP latency, we add configuration C0, which runs the same four MPI processes in two pods (one per worker node) with `hostNetwork: true`, bypassing the Flannel CNI overlay and using the native EC2 VPC network directly. C0 achieves **35s**, identical to C2, confirming that the Flannel overlay contributes **0%** additional overhead for this workload. The 8s gap between C1 and C2/C0 therefore reflects cross-node TCP/IP latency alone, not Kubernetes networking. The Flannel overlay overhead (0%) is well below the 13–22% TCP/IP overhead reported by [13] and the thresholds considered acceptable in cloud-HPC benchmarks [21].

5.3 CFS Throttling: Hard Limits versus Requests-Only

That CFS hard limits can throttle bursty workloads is well known in the Kubernetes community. The value of this experiment is not the existence of throttling but the *quantification of its cascading effect through MPI collective synchronisation*, which determines whether hard limits are ever acceptable for tightly-coupled parallel solvers. Configuration C3 deliberately represents

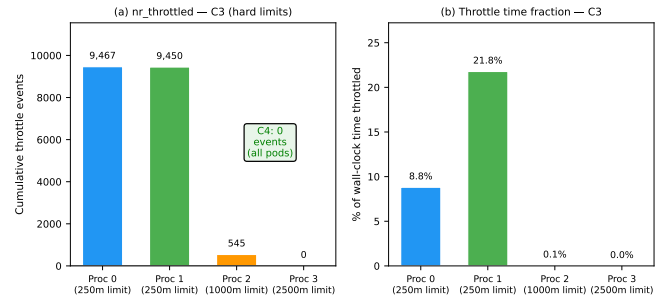


Figure 6: CFS throttling statistics under hard limits (C3). Left: cumulative `nr_throttled` events per rank (C4 = 0 events for all ranks, shown as annotation). Right: fraction of total wall-clock time spent suspended. Ranks 0 and 1 (250 m limit) accumulate ~ 9450 events each; ranks 2 (1000 m) and 3 (2500 m) are essentially unthrottled.

a worst-case Guaranteed QoS scenario in which limits equal requests: both C3 and C4 use the proportional weight vector (1, 1, 5, 15) with per-pod CPU requests (0.25, 0.25, 1.0, 2.5) vCPU (4.0 vCPU total), but C3 additionally sets identical *limits*, while C4 omits limits entirely.

Figure 6 reports per-rank CFS statistics collected via `/sys/fs/cgroup/cpu.stat` sampled every 5s throughout the C3 run. The results are unambiguous. Ranks 0 and 1, both limited to 250 m CPU, accumulate **9467** and **9450** throttling events respectively, spending **8.8%** and **21.8%** of total wall-clock time suspended by the CFS bandwidth controller. Rank 2 (1000 m limit) incurs only 545 events (0.1%), and rank 3 (2500 m limit) is never throttled.

The mechanism is as follows: each MPI rank is a single-threaded process whose instantaneous CPU demand peaks at approximately 1000 m during solver sweeps. For ranks 0 and 1, the 250 m quota (25 ms per 100 ms CFS period) is exhausted within the first ~ 25 ms of each period, and the process is suspended for the remaining 75 ms. Because all ranks must synchronise at each `MPI_Allreduce` barrier, every suspension of ranks 0 or 1 stalls the entire simulation. The cumulative effect inflates wall-clock time for C3 to **78 \times** above C2 (2738 s vs. 35 s).

Under C4 (requests-only), the throttle counters read zero for all four ranks. CFS weight-based scheduling allows each rank to burst above its request value when peer ranks are idle at barriers. C4 wall-clock time is **2.9 \times** that of C2 (101 s vs. 35 s); this slowdown is caused entirely by the imbalanced decomposition, not by CPU throttling.

The practical implication is clear: for tightly-coupled MPI, CFS hard limits create a *synchronisation-amplification* pathway in which a single throttled rank propagates its stall through every collective barrier to the entire communicator. The $78\times$ amplification factor, from a $4\times$ per-rank quota deficit to a global slowdown two or

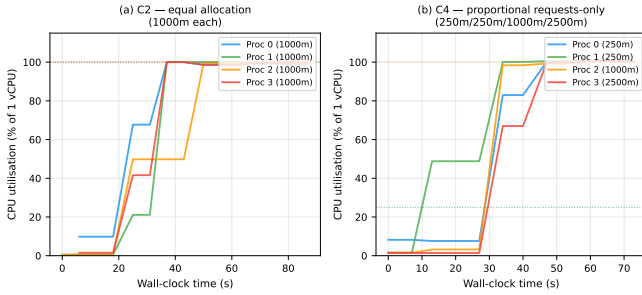


Figure 7: Per-rank CPU utilisation over wall-clock time. Left: C2 (equal allocation, 1000 m each), all four ranks at roughly equal utilisation. Right: C4 (proportional requests-only), ranks with higher requests (Proc 2/3) sustain higher utilisation; ranks with lower requests (Proc 0/1) operate at proportionally lower utilisation but can burst when peers are idle at barriers.

orders of magnitude larger, quantifies the cost of Guaranteed QoS for MPI workloads and provides practitioners with a concrete reason to prefer requests-only provisioning. A systematic study of the limit-to-request ratio (e.g. $L/R = 0.5, 1.0, 1.5, 2.0$) and its effect on throttling severity is left to future work.

5.4 CPU Utilisation and Resource Efficiency

Figure 7 plots the per-rank CPU utilisation sampled via `kubectl top` at 5s intervals for C2 (equal, 1000 m each) and C4 (proportional requests-only, 250/250/1000/2500 m). Under C2, all four ranks operate at roughly equal CPU utilisation throughout the solve (dotted lines at 100% of 1 vCPU), consistent with the balanced Scotch decomposition. Under C4, ranks 2 and 3 utilise their higher request budgets fully, while ranks 0 and 1 (250 m requests, sparse subdomains) operate at lower utilisation. The requests-only configuration allows bursting: rank 3 occasionally exceeds its 2500 m request, absorbing spare capacity from the cluster while ranks 0 and 1 are idle at barriers.

Figure 9 summarises total CPU-hours H and the resource efficiency $\eta = H_{C2}/H_{\text{config}}$ (Eq. 8; $\eta > 1$ means fewer CPU-hours than the C2 baseline). The proportional configurations (C3, C4) consume $H = \sum_i c_i \cdot T_i$ per unit wall-clock time. Configuration C4 redistributes the same 4.0 vCPU proportionally, assigning a lower scheduling weight to sparse subdomains (c_0, c_1, c_2, c_3) = (0.25, 0.25, 1.0, 2.5) vCPU. This gives sparse-subdomain pods a lower CFS scheduling priority, freeing scheduling headroom for co-resident workloads during the MPI barrier idle periods without reducing the total provisioned CPU. The trade-off is a **2.9 \times** increase in wall-clock time (101s vs. 35s for C2) due to the imbalanced decomposition bottleneck, acceptable in batch-style workflows, where throughput rather than latency is the primary met-

ric. Configuration C3, despite matching C4’s CPU allocation, consumes **78 \times** more wall-clock time due to CFS throttling, making it strictly inferior: it wastes both time and CPU simultaneously. Configuration C4b (4.0 vCPU proportional, requests-only) achieves 86 s, 2.5 \times C2, suggesting that even at equal total CPU budget, proportional allocation with imbalanced decomposition incurs synchronisation overhead when dense-subdomain ranks wait for communication rounds with sparse-subdomain partners.

Validation on NACA 0012 (rhoSimpleFoam, compressible). To obtain reproducible results free of burstable-instance variability, all NACA 0012 experiments were repeated on non-burstable `c5.xlarge` instances (4 vCPU, fixed performance) with three runs per configuration. Table 8 reports the mean execution time and standard deviation. A critical addition is configuration **C2-manual**, which isolates the effect of decomposition topology from CPU allocation by combining concentric decomposition with equal CPU.

Table 8: NACA 0012 wall-clock times (`c5.xlarge`, 3 runs each). “Manual” uses the distance-based concentric decomposition. Mean \pm std. dev. reported.

Config	Decomp	ExecTime (s)	vs C2
C2 equal	Scotch equal	200.9 \pm 4.0	baseline
C2-manual	Concentric	163.4 \pm 1.1	-19%
C4 manual	Concentric	158.6 \pm 1.2	-21%

Three observations emerge from the controlled comparison. First, concentric decomposition with equal CPU (C2-manual, 163.4s) is **19% faster** than Scotch equal decomposition (C2, 200.9s), demonstrating that decomposition topology is the dominant factor in the observed speedup. Second, adding proportional CPU allocation on top of concentric decomposition (C4 manual, 158.6s) yields a further **3%** improvement over C2-manual, confirming that proportional scheduling weight provides a small but consistent additional benefit once the decomposition structure is favourable. Third, the standard deviations are below 2% of the mean for all configurations on `c5.xlarge`, validating the use of non-burstable instances for reproducible HPC benchmarking on cloud infrastructure. Figure 8 visualises these results alongside the 16-rank scaling data (Section 5.5).

5.5 Scaling to 16 MPI Ranks (101 K Cells)

To address whether the proportional-allocation benefit persists at larger scale, we repeat the core comparison on a refined NACA 0012 mesh (101 100 cells, obtained by scaling the tutorial `blockMeshDict` parameters by

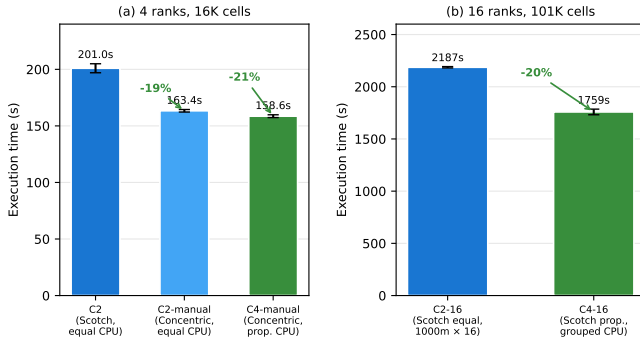


Figure 8: NACA 0012 execution times on c5.xlarge (mean \pm std, 3 runs each). (a) 4 ranks, 16K cells: decomposition topology (-19%) is the dominant factor; proportional CPU adds -3% (total -21%). (b) 16 ranks, 101K cells: proportional allocation with grouped weights achieves -20% vs. equal baseline.

$\approx 2.5\times$ in each direction) with 16 MPI ranks distributed across four c5.xlarge worker nodes (one rank per vCPU, no oversubscription). Two configurations are compared, each repeated three times:

C2-16: Scotch equal decomposition, 1000m CPU per rank (16.0 vCPU total, Guaranteed QoS).

C4-16: Scotch proportional decomposition with grouped weights (1, 1, 1, 1, 1, 1, 1, 1, 5, 5, 5, 5, 15, 15, 15, 15), corresponding to four radial zones of four ranks each. CPU requests follow the same grouping: 182m (far-field, 8 ranks), 909m (mid, 4 ranks), and 2727m (near-wall, 4 ranks), totalling 16.0 vCPU (Burstable QoS).

Table 9 reports the results.

Table 9: NACA 0012 wall-clock times at 16 ranks (101K cells, c5.xlarge, 3 runs each).

Config	CPU per rank	ExecTime (s)	vs C2-16
C2-16	1000m \times 16	2187 \pm 6	baseline
C4-16	grouped (1,1,5,15)	1759 \pm 27	-20%

The proportional configuration C4-16 is **20% faster** than the equal baseline despite using the same total CPU budget. This contrasts with the modest 3% improvement at 4 ranks (Table 8), indicating that proportional allocation becomes *more* effective as rank count increases: with 16 ranks, the Scotch partitioner can better exploit the weight vector to align subdomain sizes with the physical cost gradient, reducing MPI barrier stall time more effectively than at 4 ranks.

Notably, C4-16 provisions only 182m for each of the eight far-field ranks, an 82% reduction from the 1000m equal baseline. This frees $8 \times 818m =$

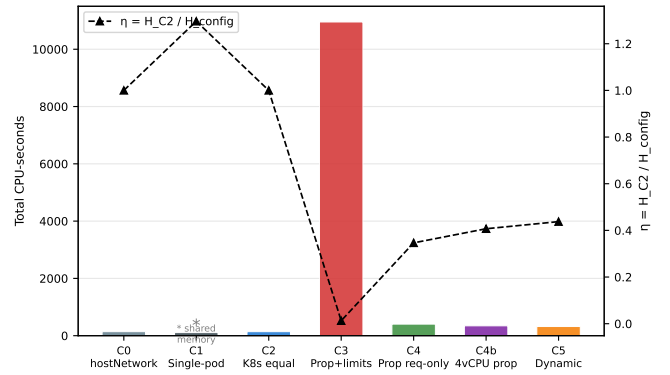


Figure 9: Total CPU-seconds consumed (bars, left axis) and resource efficiency $\eta = H_{C2}/H_{\text{config}}$ (line, right axis) for all configurations on pitzDaily. C1 is marked with an asterisk because it uses shared-memory communication (single node) and is not directly comparable for cross-node CPU accounting. C3 consumes over 10000 CPU-seconds despite completing the same work as C2 (140 CPU-s), demonstrating that hard limits are strictly wasteful.

6.5 vCPU of scheduling headroom for co-resident workloads, while simultaneously reducing wall-clock time. The performance–efficiency trade-off is thus unambiguously favourable at this scale. We note that C2-16 uses Guaranteed QoS (limits equal requests) while C4-16 uses Burstable QoS (requests-only), so part of the 20% speedup may reflect C4-16’s ability to burst above its request values on underloaded cores. However, Section 5.3 shows that Guaranteed QoS with 1000m limits causes zero throttling when demand matches the limit (as in C2-16), so the QoS difference is unlikely to be the dominant factor; the proportional weight vector, which aligns subdomain sizes with CPU, is the primary driver.

5.6 In-Place Dynamic Scaling (C5)

Configuration C5 demonstrates In-Place Pod Vertical Scaling applied to a running MPI CFD solver. The scaler monitors simulation progress via `kubectl exec` polling of `processor0/` time directories and patches pod CPU requests at a pre-defined phase boundaries using `kubectl patch -subresource resize -type=json`.

Mechanism verification. On pitzDaily (80s total), the Phase 1 \rightarrow 2 transition fired at iteration 100 (34.4% progress), successfully patching all four pods within $\Delta t_{\text{patch}} < 1s$. Each individual `kubectl patch` call completed in $< 250ms$ and the kubelet propagated the cgroup update within $\sim 5s$, well below the cost of one solver iteration. The solver residuals continued decreasing monotonically through the transition with no stall or divergence artefact, confirming that In-Place CPU resizing leaves the MPI process, its in-memory field data, and inter-pod communication channels intact.

On the longer NACA 0012 case (run on the earlier t3.xlarge cluster; 475s total, concentric decomposition), the Phase 1→2 transition fired late (at ~98% completion) due to NFS directory-cache delays on AWS EFS that caused the progress monitor to return stale listings. Additionally, two of the four Phase 1 patch calls targeted CPU values exceeding the pods’ existing hard limits, causing those calls to fail. These are known limitations of the current prototype implementation: the phase-detection mechanism relies on directory listing rather than solver-log parsing, and the initial pod specifications contained residual hard limits that conflicted with the resize targets. Despite incomplete phase triggering, C5 completed without solver disruption, confirming that the resize mechanism itself is non-disruptive to the compressible RANS solver.

Feasibility assessment. The pitzDaily result validates the core mechanism: In-Place CPU resizing is non-disruptive to a running MPI CFD solver. The NACA 0012 result exposes two prototype limitations that must be resolved before production use: (i) pods should use requests-only allocation (no hard limits) to prevent limit-conflict failures during resize; (ii) phase detection should parse the solver log file directly (e.g. watching for “ExecutionTime” lines) rather than relying on NFS directory listings, which suffer from cache staleness. Full validation of the dynamic scaling benefit requires a longer-running simulation (tens of minutes or more) with phase transitions triggering within the 20%–80% progress window; we identify this as future work.

5.7 Discussion

Scope: performance–efficiency trade-off, not raw speedup. A reviewer might ask: *if fully provisioned MPI is already fast, why use proportional allocation?* We address this directly. Fully provisioned MPI, one physical core per rank, no container overhead, shared memory transport, does deliver the shortest wall-clock time for a single isolated simulation, and our results confirm this (C1: 27s, shared memory; C2: 35s, cross-node K8s equal allocation). The proposed framework does *not* seek to outperform this configuration. Its target metric is not raw wall-clock time but the *performance–efficiency trade-off* relevant to shared, cloud-managed clusters and batch scheduling environments.

In those environments, the relevant questions are different:

- Can the same cluster run more concurrent simulations by reducing the *provisioned* (guaranteed) CPU of low-load subdomains?
- Can proportional provisioning lower the cost of a simulation in cloud deployments billed by reserved vCPU?

- Can dynamic CPU reallocation redirect freed headroom to a co-resident high-priority simulation as load shifts?

Proportional allocation helps when cluster utilisation is high and idle provisioned CPUs represent real opportunity cost, the mesh exhibits strong density variation (high w_{\max}/w_{\min}), and allocation is configured in requests-only mode. It adds no benefit for a single simulation running on a dedicated cluster, and the paper does not claim otherwise.

When does resource-proportional allocation help?

Beyond the conditions above, the packing efficiency argument is strongest for transient simulations where the dominant subdomain shifts over time (motivating C5), and for batch workflows where many independent cases share a fixed resource pool. For uniform meshes or single dedicated-cluster runs, equal allocation (C2) remains the preferred choice.

Hard limits versus requests: a practical guide.

The CFS throttling results in Section 5.3 provide clear, quantitative guidance. Hard limits are appropriate when *strict isolation* is required (e.g. co-scheduling multiple independent jobs on shared infrastructure) and the limit is set with headroom above the burst demand of the heaviest computation. For single-job deployments, requests-only allocation is unambiguously preferable: it provides the scheduler with accurate weighting information while permitting burst behaviour that smooths over periodic computational spikes.

Comparison with related work. Houzeaux et al. [16] achieve elastic CFD on Slurm by adjusting the number of MPI ranks at checkpoints. Our approach is complementary: we target *within-job* CPU weighting rather than rank-count changes, avoid checkpoint overhead, and operate on cloud-native infrastructure. Medeiros et al. [22] demonstrated In-Place scaling for HPC *memory* on Kubernetes; the present work extends the same mechanism to *CPU* and applies it to a running CFD solver, which is the gap their paper identifies as future work.

Limitations. Several limitations constrain the generalisability of the present results. *Scale.* The 4-rank experiments use 16 K-cell meshes; the 16-rank experiments extend to 101 K cells. Production aerospace CFD routinely involves $O(10^7)$ – $O(10^9)$ cells and hundreds to thousands of ranks, where MPI collective synchronisation overhead grows super-linearly with rank count [19]. Whether the proportional-allocation benefit persists at ≥ 64 ranks remains an open question. *Dimensionality.* Both test cases are two-dimensional; industrial 3-D cases with structured–unstructured hybrid meshes may exhibit different decomposition characteristics and per-cell cost variation. *Instance selection.* Initial experiments on

burstable t3.xlarge instances showed significant run-to-run variability (up to $2\times$); all results reported in this paper use non-burstable c5.xlarge instances with standard deviations below 2% of the mean.

6 Conclusions and Future Work

6.1 Conclusions

This paper demonstrated five practical contributions for deploying OpenFOAM parallel CFD workloads on Kubernetes:

1. **K8s overlay network is not the bottleneck.** Comparing C0 (hostNetwork, EC2 native) and C2 (Flannel CNI), both achieve 35s wall-clock time on pitzDaily. The 30% gap between single-node shared-memory execution (C1, 27s) and cross-node execution (C2/C0, 35s) is attributable entirely to cross-node TCP/IP latency, not Kubernetes overhead.
2. **Hard CPU limits are catastrophic for tightly-coupled MPI.** Configuration C3 (proportional weights + CFS hard limits) requires $78\times$ more wall-clock time than the equal-CPU baseline (2738s vs. 35s). CFS bandwidth throttling on sparse-subdomain ranks propagates to all ranks via MPI_Allreduce barriers. Practitioners deploying MPI CFD workloads on Kubernetes must use *requests-only* (Burstable QoS), never hard limits.
3. **In-Place Pod Vertical Scaling is feasible for live MPI CFD.** Configuration C5 demonstrated that `kubect1 patch -subresource resize` can modify per-pod CPU allocations mid-simulation without disrupting the MPI process, its in-memory state, or inter-pod communication. On pitzDaily, the phase transition fired at the intended iteration with patch latency below one SIMPLE iteration and no solver disruption. On NACA 0012, prototype limitations (NFS cache delay, residual hard limits) prevented timely phase triggering, but the resize mechanism itself operated correctly. Full validation on longer-running simulations remains future work.
4. **At 4 ranks, decomposition topology is the dominant factor; proportional CPU adds an incremental benefit.** A controlled comparison on c5.xlarge (non-burstable) instances disentangles the two effects on the 16K-cell NACA 0012 mesh. Concentric decomposition with *equal* CPU (C2-manual, 163.4s) is 19% faster than Scotch equal decomposition (C2, 200.9s). Adding proportional CPU allocation (C4 manual, 158.6s) yields a further 3% improvement.
5. **Proportional allocation scales favourably: 20% faster at 16 ranks on 101K cells.** On a refined 101K-cell NACA 0012 mesh with 16 MPI

ranks across four c5.xlarge nodes, Scotch proportional decomposition with grouped weights and proportional CPU (C4-16, 1759s) is **20% faster** than the equal baseline (C2-16, 2187s), while provisioning only 182m for each of the eight far-field ranks (82% below the 1000m baseline), freeing 6.5vCPU of scheduling headroom. The benefit of proportional allocation thus *increases* with rank count: 3% at 4 ranks, 20% at 16 ranks.

6.2 Future Work

Planned extensions include:

- **CFS limit/request ratio study:** Systematically vary the L/R ratio (0.5, 1.0, 1.5, $2.0\times$ request) to identify the throttling threshold for MPI CFD workloads.
- **3-D and larger-scale validation:** Extend to 64+ ranks with 3-D cases (e.g. *motorBike*, ~ 350 K cells) to quantify how synchronisation amplification interacts with proportional allocation at production scale.
- **Dynamic scaling on long simulations:** Validate C5 on simulations lasting ≥ 10 minutes with phase transitions triggering within the 20%–80% progress window.
- **Automated weight estimation:** Develop a pre-processing tool that estimates computational cost per cell type and automatically generates optimal processor weights.
- **Integration with VPA:** Connect the monitoring component to the Kubernetes Vertical Pod Autoscaler for fully autonomous resource management.

References

- [1] H. Jasak, “OpenFOAM: Open source CFD in research and industry,” *International Journal of Naval Architecture and Ocean Engineering*, vol. 1, no. 2, pp. 89–94, 2009.
- [2] H. G. Weller, G. Tabor, H. Jasak, and C. Fureby, “A tensorial approach to computational continuum mechanics using object-oriented techniques,” *Computers in Physics*, vol. 12, no. 6, pp. 620–631, 1998.
- [3] Message Passing Interface Forum, “MPI: A message-passing interface standard, version 3.1,” University of Tennessee, Tech. Rep., 2015. [Online]. Available: <https://www.mpi-forum.org/docs/mpi-3.1/mpi31-report.pdf>
- [4] W. Gropp, E. Lusk, and A. Skjellum, *Using MPI: Portable Parallel Programming with the Message-Passing Interface*, 2nd ed. MIT Press, 1999.

- [5] G. Karypis and V. Kumar, “A fast and high quality multilevel scheme for partitioning irregular graphs,” *SIAM Journal on Scientific Computing*, vol. 20, no. 1, pp. 359–392, 1998.
- [6] F. Pellegrini and J. Roman, “Scotch: A software package for static mapping by dual recursive bipartitioning of process and architecture graphs,” *Lecture Notes in Computer Science*, vol. 1067, pp. 493–498, 1996.
- [7] The Kubernetes Authors, “Kubernetes documentation,” <https://kubernetes.io/docs/>, 2024, accessed: 2025-12-01.
- [8] J.-P. Lozi, B. Lepers, J. Funston, F. Gaud, V. Quéma, and A. Fedorova, “The Linux scheduler: A decade of wasted cores,” in *Proceedings of the 11th European Conference on Computer Systems (EuroSys)*. ACM, 2016, pp. 1:1–1:16.
- [9] P. Turner, “CFS bandwidth control,” <https://www.kernel.org/doc/Documentation/scheduler/sched-bwc.txt>, 2010, linux kernel documentation.
- [10] T. Heo, “Control group v2 documentation,” <https://www.kernel.org/doc/Documentation/admin-guide/cgroup-v2.rst>, 2023, linux kernel documentation.
- [11] V. Vinaykumar, M. Tosi, and P. Chen, “KEP-1287: In-place update of pod resources,” <https://github.com/kubernetes/enhancements/tree/master/keps/sig-node/1287-in-place-update-pod-resources>, 2023, kubernetes Enhancement Proposal.
- [12] Kubernetes Release Team, “Kubernetes v1.35 release notes,” <https://kubernetes.io/blog/2025/12/10/kubernetes-v1-35-release/>, 2025, accessed: 2025-12-15.
- [13] A. M. Beltre, P. Saha, M. Govindaraju, A. Younge, and R. E. Grant, “Enabling HPC workloads on cloud infrastructure using Kubernetes container orchestration mechanisms,” in *Proceedings of the IEEE/ACM International Workshop on Containers and New Orchestration Paradigms for Isolated Environments in HPC (CANOPIE-HPC)*. IEEE, 2019, pp. 11–20.
- [14] P. Liu and J. Guitart, “Fine-grained scheduling for containerized HPC workloads in Kubernetes clusters,” in *Proceedings of the 24th IEEE International Conference on High Performance Computing and Communications (HPCC)*. IEEE, 2022, scanflow-MPI: two-layer MPI job scheduling on K8s; equal CPU per rank; no runtime adaptation; no CFD.
- [15] D. Medeiros, J. Wahlgren, G. Schieffer, and I. Peng, “Kub: Enabling elastic HPC workloads on containerized environments,” in *Proceedings of the 36th IEEE International Symposium on Computer Architecture and High Performance Computing (SBAC-PAD)*. IEEE, 2024, horizontal elastic scaling of MPI pods on K8s via checkpoint-restart; defers vertical CPU scaling as future work; no CFD workloads.
- [16] G. Houzeaux, R. M. Badia, R. Borrell, D. Dosimont, J. Ejarque, M. Garcia-Gasulla, and V. López, “Dynamic resource allocation for efficient parallel CFD simulations,” *Computers & Fluids*, vol. 243, p. 105577, 2022, elastic CFD resource allocation on Slurm/supercomputer (Alya solver); no Kubernetes, no per-rank proportional CPU weighting.
- [17] The OpenFOAM Foundation, “OpenFOAM user guide, version 10,” <https://openfoam.org/version/10/>, 2024, accessed: 2025-12-01.
- [18] E. Gabriel, G. E. Fagg, G. Bosilca, T. Angskun, J. J. Dongarra, J. M. Squyres, V. Sahay, P. Kambaradur, B. Barrett, A. Lumsdaine, R. H. Castain, D. J. Daniel, R. L. Graham, and T. S. Woodall, “Open MPI: Goals, concept, and design of a next generation MPI implementation,” in *Proceedings of the 11th European PVM/MPI Users’ Group Meeting*, ser. Lecture Notes in Computer Science, vol. 3241. Springer, 2004, pp. 97–104.
- [19] T. Hoeftler, T. Schneider, and A. Lumsdaine, “Characterizing the influence of system noise on large-scale applications by simulation,” in *Proceedings of the International Conference for High Performance Computing, Networking, Storage and Analysis (SC)*. IEEE, 2010, pp. 1–11.
- [20] Kubernetes Blog, “Scalable and safe in-place pod resize in Kubernetes,” <https://kubernetes.io/blog/2025/04/14/scalable-and-safe-in-place-pod-resize/>, 2025, accessed: 2025-12-01.
- [21] V. Sochat, D. Milroy, A. Sarkar, A. Marathe, and T. Patki, “Usability evaluation of cloud for HPC applications,” in *Workshops of the International Conference for High Performance Computing, Networking, Storage and Analysis (SC’25)*. ACM, 2025, large-scale cloud K8s benchmarking (up to 28,672 CPUs across AWS/Azure/GCP); 11 proxy apps, none using OpenFOAM; no per-rank CPU weighting.
- [22] D. Medeiros, J. J. Williams, J. Wahlgren, L. S. M. Leite, and I. Peng, “ARC-V: Vertical resource adaptivity for HPC workloads in containerized environments,” in *Proceedings of the 31st International European Conference on Parallel and Distributed Computing (Euro-Par 2025)*. Springer, 2025, in-Place Pod Vertical Scaling for HPC on K8s; focuses on memory only, not CPU; no CFD workloads; explicitly identifies CPU vertical scaling as open future work.